









Squeezing at the normal-mode splitting frequency of a nonlinear coupled cavity

Jonas Junker ^{1,2,*} Jiayi Qin ¹ Vaishali B. Adya ³ Nutsinee Kijbunchoo ⁴ Sheon S. Y. Chua ¹ Terry G. McRae ¹ Bram J. J. Slagmolen ¹ and David E. McClelland ¹

¹*OzGrav, Centre for Gravitational Astrophysics, Research School of Physics & Research School of Astronomy and Astrophysics, Australian National University, Australian Capital Territory, Australia.*
²*Center for Macroscopic Quantum States (bigQ), Department of Physics, Technical University of Denmark, 2800 Kongens Lyngby, Denmark*
³*Nonlinear and Quantum Photonics Lab, Department of Applied Physics, KTH Royal Institute of Technology, Stockholm, Sweden.*
⁴*OzGrav, University of Adelaide, Adelaide, South Australia, Australia.*
 (Dated: May 7, 2025)

Coupled optical cavities, which support normal modes, play a critical role in optical filtering, sensing, slow-light generation, and quantum state manipulation. Recent theoretical work has proposed incorporating nonlinear materials into these systems to enable novel quantum technologies. Here, we report the first experimental demonstration of squeezing generated in a quantum-enhanced coupled-cavity system, achieving a quantum noise reduction of 3.3 dB around the normal-mode splitting frequency of 7.47 MHz. We provide a comprehensive analysis of the system’s loss mechanisms and performance limitations, validating theoretical predictions. Our results underscore the promise of coupled-cavity squeezers for advanced quantum applications, including gravitational wave detection and precision sensing.

Coupled oscillators exhibit unique properties, such as the resonances of normal modes observable in simple mechanical systems like two masses connected by a spring [1]. Normal modes also arise in more complex systems, such as optomechanical oscillators [2], light-atom interactions [3, 4], and coupled cavities. These coupled oscillators exhibit a rich spectrum of interesting phenomena. For example, in quantum optomechanics, cavities with membranes or cantilevers [5], enhance displacement sensitivity [6], enable oscillator cooling [7], and exploit quantum back-action [8]. Atom-light interactions provide platforms for quantum interfaces [9] or evade quantum back-action [8].

Normal-mode splitting in coupled cavities arises from the constructive and destructive interference of optical modes. This phenomenon enables applications such as narrow-band filtering and precise mode selection [10], coupled-cavity-induced transparency [11–13], sensing [14], slow light generation [15], and manipulation of squeezed states [16]. The mode-splitting parameters depend solely on the optical properties of the cavities [17], offering high tunability, robustness for on-chip photonic solutions, and operation at room temperature.

The integration of nonlinear materials into coupled optical cavities has emerged as a promising area of research, inspiring various theoretical proposals. A key application is internal squeezing [18–26], where a nonlinear crystal is placed within the coupled cavity of a gravitational wave detector (GWD), enhancing sensitivity to events such as binary neutron star mergers detectable at the system’s normal-mode frequency [27, 28]. Other studies explore enhancing second-harmonic generation by incorporating second-order nonlinear materials into one cavity of a cou-

pled microcavity system [29]. Effects such as unconventional amplification [30] or photon blockades [31] seem to be also feasible when a nonlinear material is placed in a coupled cavity system. Most recent work suggests that squeezing can be amplified by coupling two optical cavities containing nonlinear materials [32]. However, realizing these concepts experimentally remains a critical challenge for unlocking their full potential.

We present a system consisting of a squeezing cavity coupled to an empty test cavity, measuring 3.3 dB of squeezing around the system’s normal-mode splitting frequency of 7.47 MHz. This quantum-enhanced nonlinear coupled cavity is locked by two nominally decoupled modes. Through a thorough characterization of all loss channels, we identify the setup’s challenges and limitations, such as the system’s escape efficiency and phase noise. Our measurements validate the theoretical predictions from [27], demonstrating that a coupled cavity squeezer generates squeezing at the normal-mode frequencies. This result marks an important milestone in advancing nonlinear quantum-enhanced coupled cavities, especially to enable next-generation high-frequency gravitational wave detectors. Our system could be also interesting for quantum information processing or quantum memory.

Figure 1 illustrates a conceptual coupled-cavity system consisting of a test cavity coupled to a squeezing cavity via a mirror with power reflectivity R_c . The squeezing cavity incorporates a nonlinear $\chi^{(2)}$ medium with down-conversion coupling strength $\chi \propto \chi^{(2)}$. The optical lengths of the test and squeezing cavities are L_{test} and L_{sqz} , respectively. The system’s input and output power reflectivities are R_{in} and R_{out} , respectively, and

its decay rate is denoted by γ . When the test cavity is blocked, the system reduces to the squeezing cavity alone with decay rate γ_{sqz} . Then, the output noise variances of the amplitude (+) and phase (−) quadratures, dependent on the measurement frequency ω are [33–35]

$$V_{\text{sqz}}^{\pm}(\omega) = 1 \pm \frac{4\gamma_{\text{sqz}}\chi}{(\gamma_{\text{sqz}} \mp \chi)^2 + \omega^2}. \quad (1)$$

For the coupled system, the amplitude noise transfer function to the output can be approximated as [27]

$$\mathcal{T}^{\pm}(\omega) = \frac{(\gamma \mp \chi)\omega + i(\omega^2 - \omega_s^2)}{(\gamma \pm \chi)\omega + i(\omega^2 - \omega_s^2)}, \quad (2)$$

resulting in output noise variances given by

$$V_c^{\pm}(\omega) = |\mathcal{T}^{\pm}(\omega)|^2 \quad (3)$$

$$= 1 \pm \frac{4\gamma\chi\omega^2}{(\gamma \mp \chi)^2\omega^2 + \omega^4 - 2\omega^2\omega_s^2 + \omega_s^4}. \quad (4)$$

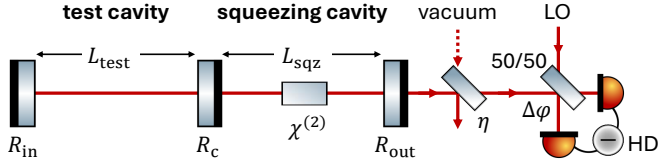


FIG. 1. Conceptual diagram of a test cavity coupled to a squeezing cavity. The squeezed output state undergoes losses of $1 - \eta$ and is directed to a balanced homodyne detector (HD), where it interferes with a local oscillator (LO) and phase noise $\Delta\varphi$ is present.

The noise variances reveal a quantum noise reduction at ω_s , the normal-mode splitting frequency resulting from the coupling between the two cavities. In the approximation of small couplings $T_c = 1 - R_c \ll 1$, this frequency depends on the optical lengths of the individual cavities and the transmissivity of the coupling mirror [36]:

$$\omega_s = c \sqrt{\frac{T_c}{4L_{\text{test}}L_{\text{sqz}}}}. \quad (5)$$

Upon exiting the coupled cavity, the quantum state experiences total optical losses of $1 - \eta$, which are described by a beam splitter process. At the beam splitter of the homodyne detector (HD), the detection angle $\Delta\varphi$ introduces additional phase noise. These two effects degrade the measured variance of the readout quadrature, with $i \in \{\text{sqz}, c\}$:

$$V_{\text{det}}^{\pm} = (V_i^{\pm} \cos^2 \Delta\varphi + V_i^{\mp} \sin^2 \Delta\varphi) \eta + 1 - \eta. \quad (6)$$

Equation (6), which accounts for phase noise, optical losses, and frequency dynamics, is used to fit the measured squeezed noise variances shown later.

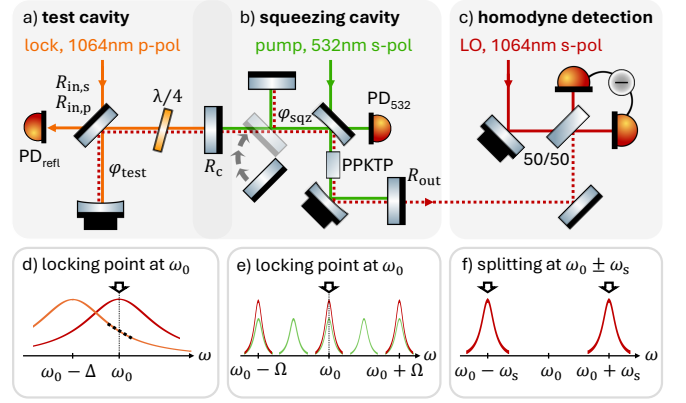


FIG. 2. Top row: Experimental setup diagram including a) the test cavity, b) the squeezing cavity and c) the homodyne detection. When the flipping mirror is up, the squeezing cavity is decoupled from the test cavity. Bottom row: Resonance responses of the three contributing modes in d) the test cavity with blue dotted error signal, e) the squeezing cavity independently, and f) the coupled oscillator's resonant modes as detected by the homodyne detector.

Our experimental setup, shown in Figure 2, comprises three main subsystems.

The first subsystem is a folded Fabry–Pérot (FP) test cavity with an effective length of $L_{\text{test}} = 1.415$ m that is stabilized using a p-polarized field. To modify the phase degeneracy between the two polarization modes, a slightly tilted quarter-wave plate is incorporated into the test cavity. The waveplate is aligned with its fast axis parallel to the cavity's polarization basis, ensuring no coupling is introduced between the polarizations. A p-polarized light field at the fundamental wavelength of $\lambda = 1064$ nm enters the test cavity through the input mirror, which has polarization-dependent power reflectivities of $R_{\text{in},s} = 99.6\%$ and $R_{\text{in},p} = 99.0\%$. The test cavity includes a high-reflective (HR) mirror that is actuated by a piezoelectric transducer (PZT) to control the cavity phase ϕ_{test} . This curved mirror is the only focusing element, setting the cavity eigenmode waist at the coupling mirror with reflectivity $R_c = 81.0\%$. The coupling mirror serves as the interface between the test cavity and the second subsystem, the squeezing cavity.

The squeezing cavity is a folded FP cavity with an optical path length of $L_{\text{sqz}} = 1.372$ m, resulting in a free spectral range (FSR) of $2\pi \times \Omega = 109.34$ MHz. This doubly-resonant cavity supports circulating fields for the s-polarised fundamental field and the pump at 532 nm, generated by an external second harmonic generation (SHG) cavity (not shown in Figure 2). Two HR curved mirrors with radii of curvature $\text{ROI} = 100$ mm are used to focus the beam into a $1 \text{ mm} \times 5 \text{ mm} \times 10 \text{ mm}$ periodically-poled potassium titanyl phosphate (PPKTP) crystal. These mirrors are hit by the beam under an angle of incidence of roughly 8° (not represented in Figure 2).

The PPKTP crystal is wedged along its 5 mm horizontal side by 1.43° and is temperature-controlled at 30°C to optimize phase-matching for efficient nonlinear down-conversion. The cavity ends with an output mirror of reflectivity $R_{\text{out}} = 90.3\%$, which couples the squeezed light out of the cavity.

An HR mirror can be flipped up to decouple the cavities and independently characterize the squeezer. This configuration preserves the squeezer's cavity length and spatial mode parameters, ensuring consistency in the optical characteristics. Characterizing the squeezing cavity by blocking the test cavity would yield an escape efficiency of $\eta_{\text{esc}} < 34\%$, making this approach unsuitable for accurate characterization.

The final subsystem is the balanced HD, which detects the squeezed state. The photodetector is an in-house design with a bandwidth of approximately 100 MHz, directly subtracting the photocurrents of the two photodiodes. The local oscillator (LO) phase is controlled using a PZT-actuated mirror, and the LO optical power is maintained at around 12 mW throughout the measurements. At this power, the homodyne detector still works linear and has a high shot noise clearance at relevant frequencies.

To generate a squeezed state at the normal-mode splitting frequency, stable locking of the entire system is essential. Normal-mode splitting occurs when both cavities are independently resonant for the fundamental frequency. The strong coupling ($T_c = 19\%$) complicates the separation of individual cavity responses. While recent methods propose using phase modulation and beat-frequency demodulation to decouple error signals [37], our approach leverages a locking technique based on two distinct modes with different wavelengths and polarizations. This method successfully decouples the systems and generates independent error signals, enabling stable locking for squeezed state generation.

The test cavity phase φ_{test} is locked using a p-polarized field at the fundamental frequency, as depicted in Figure 2d. To set the relative phase between the p- and s-polarized cavity modes Δ , we adjust the horizontal tilt of the quarter-wave plate mounted on a motorized rotation stage [Thorlabs, ELL18]. This tilt modifies the differential optical path length, thereby controlling the relative phase between the polarizations. The side-fringe slope of the cavity's p-polarized amplitude response, measured on photodetector PD_{refl} , serves as an error signal to maintain resonance for the s-polarized mode. The low finesse of the squeezing cavity for the fundamental p-polarization ensures negligible impact of the squeezer's cavity dynamics on the phase control of the test cavity. Thus the p-polarisation does not see a coupled cavity.

The squeezing cavity phase φ_{sqz} is locked with the pump field using a modulation-free polarization-based homodyne technique (indicated by PD_{532} in Figure 2) [38]. This lock is independent of the test cavity dynam-

ics due to the low intra-cavity mirror reflectivities and the HR coupling mirror for the pump. The same locking method is used when the coupling mirror is replaced by the path through the flipped-up HR mirror. The fundamental s-polarized field can be tuned to resonance by displacing the wedged birefringent crystal, adjusting the optical path length and relative phase with the pump field. Fine-tuning is achieved with small temperature changes to the crystal, which minimally affect the down-conversion phase matching.

Our locking routine allows arbitrary control of the fundamental resonance condition. For instance, the fundamental can be co-resonant (squeezing at DC and Ω), as shown in Figure 2e, or anti-resonant (squeezing at $\Omega/2$). In this plot, the green peaks are only projections for better visualization of the co-resonances. With both cavities independently locked on resonance, the coupled system enhances and correlates modes at the splitting frequency $\pm\omega_s$, as illustrated in Figure 2f.

To independently test and characterize the squeezer, we first performed a squeezing measurement by flipping the HR mirror up into the beam path. This replaced the coupling mirror, isolating the squeezer from the test cavity. For this measurement, we used 55 mW of pump power to see a fair amount of squeezing but also be sensitive to phase noise. We locked the squeezer to the pump field and set the relative phase to achieve anti-resonance for the fundamental mode. As a result, squeezing was generated at half the FSR, $\Omega/2$. At this frequency, we are neither limited by low-frequency technical noise nor by the limited bandwidth of the HD.

Because of free-running pump and detection phases, we measured 1000 spectra over a span of 10 MHz at half the FSR frequency of 54.67 MHz. To analyze the data, we selected the five spectra with the highest and lowest noise levels (grey traces) and averaged them separately (blue traces), as shown in Figure 3. We subtracted the photodetector's dark noise from the measurements and normalized the data to shot noise. To characterize the data, we fitted the model given by Equation (1) inserted into Equation (6), with $\omega_0 = \Omega/2$ to both averaged traces simultaneously (orange traces). The fit results reveal a maximum anti-squeezing of 18.9 dB above shot noise, and a minimum squeezing of 6.6 dB below shot noise. Additionally, it yields values for the total efficiency $\eta = 85.1\%$ and phase noise $\Delta\varphi = 40\text{ mrad}$. The observed phase noise is likely due to the 1.372 m-long free-space squeezer, which contains ten intra-cavity components and lacks phase-locking mechanisms. For comparison, we also plot the model function for V_{det}^- without phase noise ($\Delta\varphi = 0$, dashed orange trace). From the fitted decay rate $\gamma_{\text{sqz}} = 2\pi \times 868\text{ kHz}$ and nonlinear efficiency $\chi = 2\pi \times 704\text{ kHz}$, we calculated the squeezer's oscillation threshold as $P_{\text{thresh}} = P\gamma_{\text{sqz}}^2/\chi^2 \approx 83.7\text{ mW}$.

With the other loss channels measured independently, we performed a thorough characterization of the squeez-

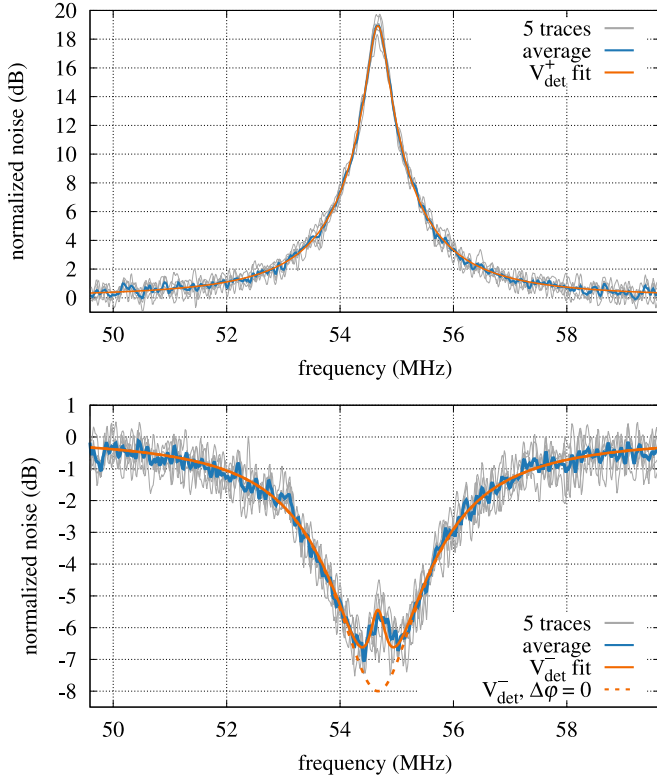


FIG. 3. Anti-squeezing (top) and squeezing (bottom) at half the FSR $\Omega/2 = 2\pi \times 54.67$ MHz, normalized to shot noise. The five measured spectra with highest and lowest noise are shown in grey. We averaged (blue traces) and fitted the data using Equation (6) (orange traces, dashed trace assumes no phase noise). At the center frequency, anti-squeezing couples into the squeezed readout quadrature because of phase noise resulting in the local maximum. The electronic dark noise, which was 12.7 dB below the shot noise, was subtracted from the noise data. Used pump power: $P = 55$ mW. The fitting parameters are: $\Delta\phi = 40$ mrad and $\eta = 85.1\%$, $\Omega = 2\pi \times 109.34$ MHz, $\chi = 2\pi \times 704$ kHz, $\gamma_{\text{sqz}} = 2\pi \times 868$ kHz.

ing setup. In separate measurements, we determined an escape efficiency of $\eta_{\text{esc}} = 97.5\%$, a propagation efficiency of $\eta_{\text{prop}} = 94.0\%$, and a homodyne efficiency of $\eta_{\text{hd}} = 94.5\%$, as summarized in Table I. Combining these efficiencies with the total efficiency from the fit, we derived a remaining loss, which we attribute to the quantum efficiency of the HD as in [39], with $\eta_{\text{qe}} = 98.2\%$. This value is consistent with the detector's gain measurements, which convert optical power into voltage.

To study the coupled system, we flipped the HR mirror down again and locked both cavities as described above. In contrast to the previous measurement, we locked the squeezer to be co-resonant with the pump field. We recorded 1000 noise spectra at the splitting frequency of 7.47 MHz with a span of 3 MHz and selected the five highest/lowest noise data sets, plotted by the grey traces in Figure 4. After subtracting dark noise and normalizing to shot noise, we again fitted the average of the five

parameter	single squeezer	coupled system
η_{esc} (%)	97.5	76.8
η_{prop} (%)	94.0	94.0
η_{hd} (%)	94.5	89.1*
η_{qe} (%)	98.2*	98.2
η (%)	85.1	63.2
$\Delta\phi$ (mrad)	40	79
anti-squeezing (dB)	18.9	14.8
squeezing (dB)	-6.6	-3.3

TABLE I. Overview of the efficiencies in the two setups. The total efficiency η and the phase noise $\Delta\phi$ are obtained from fitting the data from Figure 3 and Figure 4. Values with asterisk are inferred from the overall loss budget.

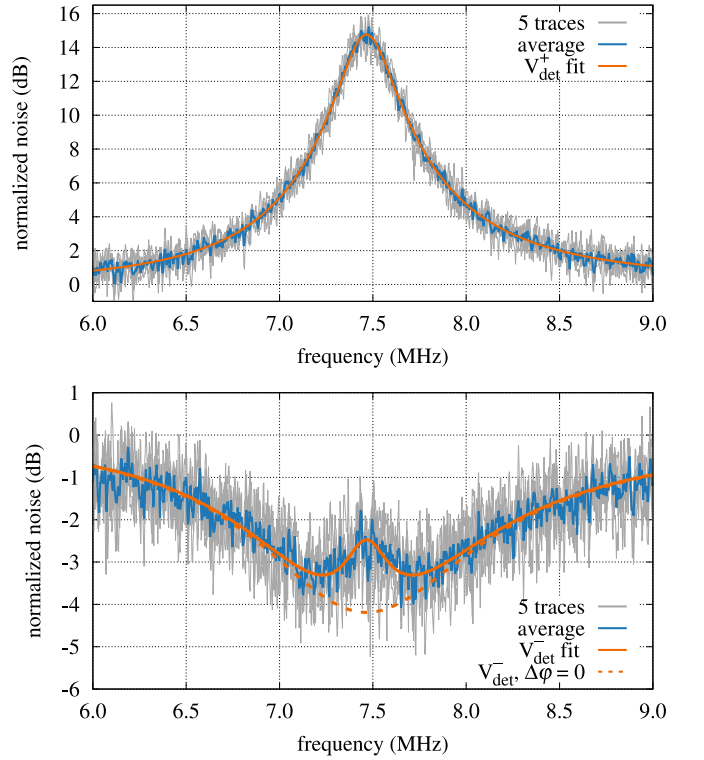


FIG. 4. Anti-squeezing (top) and squeezing (bottom) around the normal-mode splitting frequency $\omega_s = 2\pi \times 7.47$ MHz, normalized to shot noise. Measurements were taken as in Figure 3. The electronic dark noise was 13.2 dB below the shot noise and subtracted from the noise data. Used pump power: $P = 74$ mW. Fitting parameters: $\Delta\phi = 79$ mrad and $\eta = 63.2\%$, $\omega_s = 2\pi \times 7.47$ MHz, $\chi = 2\pi \times 820$ kHz, $\gamma = 2\pi \times 1.100$ MHz.

traces presented by the blue traces with the highest and lowest noise with the model in Equation (6). The fits reveal a maximum anti-squeezing of 14.8 dB above the shot noise and a minimum squeezing of 3.3 dB below the shot noise (orange traces). Additionally, the fit provided values for the total efficiency $\eta = 63.2\%$ and phase noise

$\Delta\varphi = 79$ mrad. For this measurement, we used a slightly higher pump power of $P = 74$ mW to increase the sensitivity to phase noise, enabling a more precise characterization. The phase noise during detection increased compared to the previous setup due to the coupled system incorporating more free-space optical components, which heightened its susceptibility to intra-cavity phase noise. For future experiments, improving the table's housing and implementing phase controls for both the pump and detection phases would be highly beneficial.

The noise data from the single-cavity squeezer were fitted with a nonlinear conversion efficiency of $\chi = 2\pi \times 704$ kHz, while the coupled-cavity squeezer data were fitted with $\chi = 2\pi \times 820$ kHz. This difference aligns with the different pump powers (55 mW, 74 mW), which scale with the nonlinear efficiency as $\chi \propto \sqrt{P}$. Consequently, the threshold power increased to $P_{\text{thresh}} \approx 133.1$ mW.

The overall loss budget increased due to additional losses in the coupled system and a modified homodyne contrast. The coupled setup includes new optical components, such as the quarter waveplate with losses of $L_{\text{qwp}} = 2 \times 0.8\%$, the test cavity's input-output mirror with $L_{\text{in,s}} = 2 \times 0.4\%$. The remaining losses account for $L_{\text{res}} = 0.3\%$. As a result, the escape efficiency reduced to $\eta_{\text{esc}} = 76.8\%$, consistent with the observed increase in the fitted decay rate to $\gamma = 2\pi \times 1.100$ MHz. Improving the escape efficiency would require some targeted optimizations. Employing higher-quality optical components to reduce intra-cavity losses could make an escape efficiency exceeding 90% achievable. Additionally, adopting an alternative locking scheme for the test cavity to eliminate the intra-cavity quarter waveplate could further enhance escape efficiency.

Accurately measuring the homodyne contrast is challenging due to the anti-resonance of the coupled-cavity system for the carrier field, which is a consequence of the normal mode splitting. To address this, we optimized the contrast by interfering the local oscillator with a bright field reflected from the mode-matched squeezing cavity while blocking the test cavity. However, this bright field does not perfectly match the spatial mode of the coupled-cavity field, resulting in only an approximate estimation of the homodyne contrast. For a more precise contrast, we inferred the degraded homodyne efficiency from the total loss budget, yielding $\eta_{\text{hd}} = 89.1\%$. The contrast could be improved by better matching the eigenmodes of the two cavities, ensuring that the bright field leaking from the squeezing cavity serves as a suitable reference for the squeezed field. Alternatively, a sideband at the resonant splitting frequency could be used to generate a beat note with the local oscillator at the HD.

In conclusion, we demonstrated 3.3 dB of quantum noise reduction generated by a coupled-cavity squeezer. We controlled the lengths of each cavity independently by separate polarisation and frequency modes, to generate the squeezing at the system's normal-mode splitting

frequency of 7.47 MHz. We presented a detailed analysis of the loss couplings and highlighted the associated challenges. For the characterization, we fitted our experimental data to the theory of a coupled-cavity squeezer [27], incorporating losses and phase noise in the readout. The generated squeezing is primarily limited by the system's relatively low escape efficiency of 76.8%. However, with optimizations to the cavity design and improved optical components, an escape efficiency of at least 90% should be achievable. In addition, the propagation and homodyne detection efficiencies could realistically be increased to 99% and 95%, respectively. If then the phase noise can be stabilized below 20 mrad using phase locks, the system could achieve a maximum squeezing level of 6.9 dB.

Our results highlight the feasibility of quantum-enhanced nonlinear coupled systems and are particularly important for informing future GWD designs employing the concept of internal squeezing. With the addressed optimisations, demonstrating the positive effect on the signal-to-noise-ratio for internal squeezing will be possible in this coupled system. Our system could furthermore provide valuable insights into loss couplings in coupled cavities, such as those in current GWDs LIGO [40, 41], Virgo [42] and KAGRA [43, 44]. Our insights are interesting for advanced quantum techniques related to second-harmonic generation, amplification, photon blockades and squeezing improvement. In our experiment, the sub-cavities were locked on resonance, resulting in symmetric mode splitting. We observed that detuned sub-cavities alter the generated output state, leading to frequency-dependent squeezing, similar as in [45], which warrants further exploration.

We thank Mikhail Korobko for insightful discussions and helpful remarks. We thank Daniel Gould, Dennis Wilken and Nived Johny for useful discussions and we thank Michèle Heurs from the Leibniz University Hannover for generously lending some optical components for our experiment. This research was supported by the Australian Research Council under the Discovery Grant scheme, Grant No. DP220102755. We would like to also thank the support of the Australian Research Council under the ARC Centre of Excellence for Gravitational Wave Discovery, Grants No. CE170100004, and No. CE230100016. V. B. A. would like to acknowledge the support and funding from the Swedish Research Council (VR starting Grant No. 2023-0519 and Optical Quantum Sensing environment Grant No. 201606122) and the Wallenberg Center for Quantum Technology (WACQT) in Sweden.

DATA AVAILABILITY

The data that support the plots within this paper and other findings of this study are available from the corre-

sponding author upon reasonable request.

COMPETING INTERESTS

The authors declare no competing interests.

* Corresponding author: jonju@dtu.dk

- [1] P. R. Saulson, *Phys. Rev. D* **42**, 2437 (1990).
- [2] J. M. Dobrindt, I. Wilson-Rae, and T. J. Kippenberg, *Phys. Rev. Lett.* **101**, 263602 (2008).
- [3] R. J. Thompson, G. Rempe, and H. J. Kimble, *Phys. Rev. Lett.* **68**, 1132 (1992).
- [4] A. Frisk Kockum, A. Miranowicz, S. De Liberato, S. Savasta, and F. Nori, *Nat Rev Phys* **1**, 19 (2019).
- [5] M. Aspelmeyer, T. J. Kippenberg, and F. Marquardt, *Rev. Mod. Phys.* **86**, 1391 (2014).
- [6] J. M. Dobrindt and T. J. Kippenberg, *Phys. Rev. Lett.* **104**, 033901 (2010).
- [7] J. Chan, T. P. M. Alegre, A. H. Safavi-Naeini, J. T. Hill, A. Krause, S. Gröblacher, M. Aspelmeyer, and O. Painter, *Nature* **478**, 89 (2011).
- [8] C. B. Møller, R. A. Thomas, G. Vasilakis, E. Zeuthen, Y. Tsaturyan, M. Balabas, K. Jensen, A. Schliesser, K. Hammerer, and E. S. Polzik, *Nature* **547**, 191 (2017).
- [9] K. Hammerer, A. S. Sørensen, and E. S. Polzik, *Rev. Mod. Phys.* **82**, 1041 (2010).
- [10] H. Lu, X. Liu, G. Wang, and D. Mao, *Nanotechnology* **23**, 444003 (2012).
- [11] D. D. Smith, H. Chang, K. A. Fuller, A. T. Rosenberger, and R. W. Boyd, *Phys. Rev. A* **69**, 063804 (2004).
- [12] C. Zheng, X. Jiang, S. Hua, L. Chang, G. Li, H. Fan, and M. Xiao, *Opt. Express*, OE **20**, 18319 (2012).
- [13] S.-T. Guo, Y.-H. Zhang, L.-L. Wu, M.-Y. Ye, and X.-M. Lin, *Phys. Rev. A* **103**, 033510 (2021).
- [14] G. C. Righini and S. Soria, *Sensors* **16**, 905 (2016).
- [15] K. Totsuka, N. Kobayashi, and M. Tomita, *Phys. Rev. Lett.* **98**, 213904 (2007).
- [16] K. Di, C. Xie, and J. Zhang, *Phys. Rev. Lett.* **106**, 153602 (2011).
- [17] Q. Li, T. Wang, Y. Su, M. Yan, and M. Qiu, *Opt. Express*, OE **18**, 8367 (2010).
- [18] M. Korobko, J. Südbeck, S. Steinlechner, and R. Schnabel, *Phys. Rev. A* **108**, 063705 (2023).
- [19] J. W. Gardner, M. J. Yap, V. Adya, S. Chua, B. J. J. Slagmolen, and D. E. McClelland, *Phys. Rev. D* **106**, L041101 (2022).
- [20] K. Somiya, Y. Kataoka, J. Kato, N. Saito, and K. Yano, *Physics Letters A* **380**, 521 (2016).
- [21] H. Miao, N. D. Smith, and M. Evans, *Phys. Rev. X* **9**, 011053 (2019).
- [22] H. Rehbein, J. Harms, R. Schnabel, and K. Danzmann, *Phys. Rev. Lett.* **95**, 193001 (2005).
- [23] V. Peano, H. G. L. Schwefel, Ch. Marquardt, and F. Marquardt, *Phys. Rev. Lett.* **115**, 243603 (2015).
- [24] M. Korobko, L. Kleybolte, S. Ast, H. Miao, Y. Chen, and R. Schnabel, *Phys. Rev. Lett.* **118**, 143601 (2017).
- [25] M. Korobko, J. Südbeck, S. Steinlechner, and R. Schnabel, *Phys. Rev. Lett.* **131**, 143603 (2023).
- [26] N. Böttner, J. Bentley, R. Schnabel, and M. Korobko, *Phys. Rev. D* **110**, 103010 (2024).
- [27] M. Korobko, Y. Ma, Y. Chen, and R. Schnabel, *Light Sci Appl* **8**, 118 (2019).
- [28] V. B. Adya, M. J. Yap, D. Töyrä, T. G. McRae, P. A. Altin, L. K. Sarre, M. Meijerink, N. Kijbunchoo, B. J. J. Slagmolen, R. L. Ward, and D. E. McClelland, *Class. Quantum Grav.* **37**, 07LT02 (2020).
- [29] X.-X. Lv, T.-J. Wang, and C. Wang, *Int J Theor Phys* **61**, 3 (2022).
- [30] W. C.-W. Huang and H. Batelaan, *EPL* **119**, 24002 (2017).
- [31] J.-S. Liu, J.-Y. Yang, H.-Y. Liu, and A.-D. Zhu, *Opt. Express* **28**, 18397 (2020).
- [32] H. Jabri and H. Eleuch, *Sci Rep* **14**, 7753 (2024).
- [33] D. F. Walls and G. J. Milburn, *Quantum Optics*, 2nd ed., Springer eBook Collection (Springer Berlin Heidelberg, Berlin, Heidelberg, 2008).
- [34] M. J. Collett and C. W. Gardiner, *Phys. Rev. A* **30**, 1386 (1984).
- [35] M. J. Collett and D. F. Walls, *Phys. Rev. A* **32**, 2887 (1985).
- [36] G. de Vine, M. Gray, D. E. McClelland, Y. Chen, and S. Whitcomb, *Physics Letters A* **316**, 17 (2003).
- [37] R. Maggiore, A. Freise, A. Dmitriev, and M. Sallé, *Phys. Rev. D* **109**, 022010 (2024).
- [38] T. W. Hansch and B. Couillaud, *Optics Communications* **35**, 441 (1980).
- [39] H. Vahlbruch, M. Mehmet, K. Danzmann, and R. Schnabel, *Phys. Rev. Lett.* **117**, 110801 (2016).
- [40] The LIGO Scientific Collaboration, *Class. Quantum Grav.* **32**, 074001 (2015).
- [41] LIGO O4 Detector Collaboration, D. Ganapathy, W. Jia, M. Nakano, V. Xu, N. Aritomi, T. Cullen, N. Kijbunchoo, S. E. Dwyer, A. Mullavey, L. McCuller, R. Abbott, I. Abouelfettouh, R. X. Adhikari, A. Ananyeva, S. Appert, K. Arai, S. M. Aston, M. Ball, S. W. Ballmer, D. Barker, L. Barsotti, B. K. Berger, J. Betzwieser, D. Bhattacharjee, G. Billingsley, S. Biscans, N. Bode, E. Bonilla, V. Bossilkov, A. Branch, A. F. Brooks, D. D. Brown, J. Bryant, C. Cahillane, H. Cao, E. Capote, F. Clara, J. Collins, C. M. Compton, R. Cottingham, D. C. Coyne, R. Crouch, J. Csizmazia, L. P. Dartez, N. Demos, E. Dohmen, J. C. Driggers, A. Effler, A. Ejlli, T. Etzel, M. Evans, J. Feicht, R. Frey, W. Frischhertz, P. Fritschel, V. V. Frolov, P. Fulda, M. Fyffe, B. Gateley, J. A. Giaime, K. D. Giardina, J. Glanzer, E. Goetz, R. Goetz, A. W. Goodwin-Jones, S. Gras, C. Gray, D. Griffith, H. Grote, T. Guidry, E. D. Hall, J. Hanks, J. Hanson, M. C. Heintze, A. F. Helmling-Cornell, N. A. Holland, D. Hoyland, H. Y. Huang, Y. Inoue, A. L. James, A. Jennings, S. Karat, S. Karki, M. Kasprzak, K. Kawabe, P. J. King, J. S. Kissel, K. Komori, A. Kontos, R. Kumar, K. Kuns, M. Landry, B. Lantz, M. Laxen, K. Lee, M. Lesovsky, F. Llamas, M. Lormand, H. A. Loughlin, R. Macas, M. MacInnis, C. N. Makarew, B. Mannix, G. L. Mansell, R. M. Martin, K. Mason, F. Matichard, N. Mavalvala, N. Maxwell, G. McCarrol, R. McCarthy, D. E. McClelland, S. McCormick, T. McRae, F. Mera, E. L. Merilh, F. Meylahn, R. Mittleman, D. Moraru, G. Moreno, T. J. N. Nelson, A. Neunzert, J. Notte, J. Oberling, T. O'Hanlon, C. Osthelder, D. J. Ottaway, H. Overmier, W. Parker, A. Pele, H. Pham, M. Pirello, V. Quetschke,

- K. E. Ramirez, J. Reyes, J. W. Richardson, M. Robinson, J. G. Rollins, C. L. Romel, J. H. Romie, M. P. Ross, K. Ryan, T. Sadecki, A. Sanchez, E. J. Sanchez, L. E. Sanchez, R. L. Savage, D. Schaetzel, M. G. Schiowski, R. Schnabel, R. M. S. Schofield, E. Schwartz, D. Sellers, T. Shaffer, R. W. Short, D. Sigg, B. J. J. Slagmolen, C. Soike, S. Soni, V. Srivastava, L. Sun, D. B. Tanner, M. Thomas, P. Thomas, K. A. Thorne, C. I. Torrie, G. Traylor, A. S. Ubhi, G. Vajente, J. Vanosky, A. Vecchio, P. J. Veitch, A. M. Vibhute, E. R. G. von Reis, J. Warner, B. Weaver, R. Weiss, C. Whittle, B. Willke, C. C. Wipf, H. Yamamoto, L. Zhang, and M. E. Zucker, *Phys. Rev. X* **13**, 041021 (2023).
- [42] F. Acernese, M. Agathos, K. Agatsuma, D. Aisa, N. Allemandou, A. Allocca, J. Amarni, P. Astone, G. Balestri, G. Ballardín, F. Barone, J.-P. Baronick, M. Barsuglia, A. Basti, F. Basti, T. S. Bauer, V. Bavigadda, M. Bejger, M. G. Beker, C. Belczynski, D. Bersanetti, A. Bertolini, M. Bitossi, M. A. Bizouard, S. Bloemen, M. Blom, M. Boer, G. Bogaert, D. Bondi, F. Bondu, L. Bonelli, R. Bonnand, V. Boschi, L. Bosi, T. Bouedo, C. Bradaschia, M. Branchesi, T. Briant, A. Brillet, V. Brisson, T. Bulik, H. J. Bulten, D. Buskulic, C. Buy, G. Cagnoli, E. Calloni, C. Campeggi, B. Canuel, F. Carbognani, F. Cavalier, R. Cavalieri, G. Cella, E. Cesarini, E. C. Mottin, A. Chincarini, A. Chiummo, S. Chua, F. Cleva, E. Coccia, P.-F. Cohadon, A. Colla, M. Colombini, A. Conte, J.-P. Coulon, E. Cuoco, A. Dalmaz, S. D'Antonio, V. Dattilo, M. Davier, R. Day, G. Debreczeni, J. Degallaix, S. Deléglise, W. D. Pozzo, H. Dereli, R. D. Rosa, L. D. Fiore, A. D. Lieto, A. D. Virgilio, M. Doets, V. Dolique, M. Drago, M. Ducrot, G. Endrőczy, V. Fafone, S. Farinon, I. Ferrante, F. Ferrini, F. Fidecaro, I. Fiori, R. Flaminio, J.-D. Fournier, S. Franco, S. Frasca, F. Frasconi, L. Gamaitoni, F. Garufi, M. Gaspard, A. Gatto, G. Gemme, B. Gendre, E. Genin, A. Gennai, S. Ghosh, L. Giacobbone, A. Giazotto, R. Gouaty, M. Granata, G. Greco, P. Groot, G. M. Guidi, J. Harms, A. Heidmann, H. Heitmann, P. Hello, G. Hemming, E. Hennes, D. Hofman, P. Jaranowski, R. J. G. Jonker, M. Kasprzak, F. Kéfélian, I. Kowalska, M. Kraan, A. Królak, A. Kutynia, C. Lazzaro, M. Leonardi, N. Leroy, N. Letendre, T. G. F. Li, B. Lieunard, M. Lorenzini, V. Lorette, G. Losurdo, C. Magazzù, E. Majorana, I. Maksimovic, V. Malvezzi, N. Man, V. Mangano, M. Mantovani, F. Marchesoni, F. Marion, J. Marque, F. Martelli, L. Martellini, A. Masserot, D. Meacher, J. Meidam, F. Mezzani, C. Michel, L. Milano, Y. Minenkov, A. Moggi, M. Mohan, M. Montani, N. Morgado, B. Mours, F. Mul, M. F. Nagy, I. Nardecchia, L. Naticchioni, G. Nelemans, I. Neri, M. Neri, F. Nocera, E. Pacaud, C. Palomba, F. Paoletti, A. Paoli, A. Pasqualetti, R. Passaquieti, D. Pasuello, M. Perciballi, S. Petit, M. Pichot, F. Piergiovanni, G. Pillant, A. Piluso, L. Pinard, R. Poggiani, M. Prijatelj, G. A. Prodi, M. Punturo, P. Puppo, D. S. Rabeling, I. Rácz, P. Rapagnani, M. Razzano, V. Re, T. Regimbau, F. Ricci, F. Robinet, A. Rocchi, L. Roland, R. Romano, D. Rosińska, P. Ruggi, E. Saracco, B. Sassolas, F. Schimmel, D. Sentenac, V. Sequino, S. Shah, K. Siellez, N. Straniero, B. Swinkels, M. Tacca, M. Tonelli, F. Travasso, M. Turconi, G. Vajente, N. van Bakel, M. van Beuzekom, J. F. J. van den Brand, C. V. D. Broeck, M. V. van der Sluys, J. van Heijningen, M. Vasúth, G. Vedovato, J. Veitch, D. Verkindt, F. Vetrano, A. Viceré, J.-Y. Vinet, G. Visser, H. Vocca, R. Ward, M. Was, L.-W. Wei, M. Yvert, A. Z. Żny, and J.-P. Zendri, *Class. Quantum Grav.* **32**, 024001 (2014).
- [43] T. Akutsu, M. Ando, K. Arai, Y. Arai, S. Araki, A. Araya, N. Aritomi, Y. Aso, S. Bae, Y. Bae, L. Baiotti, R. Bajpai, M. A. Barton, K. Cannon, E. Capocasa, M. Chan, C. Chen, K. Chen, Y. Chen, H. Chu, Y. K. Chu, S. Eguchi, Y. Enomoto, R. Flaminio, Y. Fujii, M. Fukunaga, M. Fukushima, G. Ge, A. Hagiwara, S. Haino, K. Hasegawa, H. Hayakawa, K. Hayama, Y. Himemoto, Y. Hiranuma, N. Hirata, E. Hirose, Z. Hong, B. H. Hsieh, C. Z. Huang, P. Huang, Y. Huang, B. Ikenoue, S. Imam, K. Inayoshi, Y. Inoue, K. Ioka, Y. Itoh, K. Izumi, K. Jung, P. Jung, T. Kajita, M. Kamiizumi, N. Kanda, G. Kang, K. Kawaguchi, N. Kawai, T. Kawasaki, C. Kim, J. C. Kim, W. S. Kim, Y. M. Kim, N. Kimura, N. Kita, H. Kitazawa, Y. Kojima, K. Kokeyama, K. Komori, A. K. H. Kong, K. Kotake, C. Kozakai, R. Kozu, R. Kumar, J. Kume, C. Kuo, H. S. Kuo, S. Kuroyanagi, K. Kusayanagi, K. Kwak, H. K. Lee, H. W. Lee, R. Lee, M. Leonardi, L. C. C. Lin, C. Y. Lin, F. L. Lin, G. C. Liu, L. W. Luo, M. Marchio, Y. Michimura, N. Mio, O. Miyakawa, A. Miyamoto, Y. Miyazaki, K. Miyo, S. Miyoki, S. Morisaki, Y. Moriwaki, K. Nagano, S. Nagano, K. Nakamura, H. Nakano, M. Nakano, R. Nakashima, T. Narikawa, R. Negishi, W. T. Ni, A. Nishizawa, Y. Obuchi, W. Ogaki, J. J. Oh, S. H. Oh, M. Ohashi, N. Ohishi, M. Ohkawa, K. Okutomi, K. Oohara, C. P. Ooi, S. Oshino, K. Pan, H. Pang, J. Park, F. E. P. Arellano, I. Pinto, N. Sago, S. Saito, Y. Saito, K. Sakai, Y. Sakai, Y. Sakuno, S. Sato, T. Sato, T. Sawada, T. Sekiguchi, Y. Sekiguchi, S. Shibagaki, R. Shimizu, T. Shimoda, K. Shimode, H. Shinkai, T. Shishido, A. Shoda, K. Somiya, E. J. Son, H. Sotani, R. Sugimoto, T. Suzuki, T. Suzuki, H. Tagoshi, H. Takahashi, R. Takahashi, A. Takamori, S. Takano, H. Takeda, M. Takeda, H. Tanaka, K. Tanaka, K. Tanaka, T. Tanaka, T. Tanaka, S. Tanioka, E. N. Tapia San Martin, S. Telada, T. Tomaru, Y. Tomigami, T. Tomura, F. Travasso, L. Trozzo, T. Tsang, K. Tsubono, S. Tsuchida, T. Tsuzuki, D. Tuyenbayev, N. Uchikata, T. Uchiyama, A. Ueda, T. Uehara, K. Ueno, G. Ueshima, F. Uraguchi, T. Ushiba, M. H. P. M. van Putten, H. Vocca, J. Wang, C. Wu, H. Wu, S. Wu, W.-R. Xu, T. Yamada, K. Yamamoto, K. Yamamoto, T. Yamamoto, K. Yokogawa, J. Yokoyama, T. Yokozawa, T. Yoshioka, H. Yuzurihara, S. Zeidler, Y. Zhao, and Z. H. Zhu, *Progress of Theoretical and Experimental Physics* **2021**, 05A101 (2021).
- [44] The KAGRA Collaboration, Y. Aso, Y. Michimura, K. Somiya, M. Ando, O. Miyakawa, T. Sekiguchi, D. Tatsumi, and H. Yamamoto, *Phys. Rev. D* **88**, 043007 (2013).
- [45] J. Junker, D. Wilken, N. Johny, D. Steinmeyer, and M. Heurs, *Phys. Rev. Lett.* **129**, 033602 (2022).